Electronic Supplementary Material (ESI) for Nanoscale.

Supplementary Information

Vacancy Engineering of Two-dimensional W_2N_3 Nanosheets for Efficient CO_2 Hydrogenation

Bin Li, [a] *Bo Ma,* [a] *Shu-Yan Wang,* [a] *Ming-Ming Yu,* [a] *Ze-Qi Zhang,* [a] *Ming-Jun Xiao,* [a] *Hong Zhang,* [b] *Jian-Feng Wu,* [a*] *Yong Peng,* [b] *Qiang Wang,* [a *] *and Hao-Li Zhang* [a *]

[a] State Key Laboratory of Applied Organic Chemistry (SKLAOC), Key Laboratory of Nonferrous Metal Chemistry and Resources Utilization of Gansu Province, College of Chemistry and Chemical Engineering, Key Laboratory of Special Function Materials and Structure Design, Ministry of Education, Lanzhou University, Lanzhou, 730000, China

[b] Electron Microscopy Centre of Lanzhou University and Key Laboratory for Magnetism and Magnetic Materials of Ministry of Education, Lanzhou University, Lanzhou 730000, China

Corresponding Author

* E-mail: qiangwang@lzu.edu.cn (Q.W.)

* E-mail: haoli.zhang@lzu.edu.cn (H.L.Z.)

* E-mail: wjf@lzu.edu.cn (J.F.W)

Materials and methods

Materials

Sodium nitrate was purchased from Tianjin Damao Chemical Reagent Factory. Ammonium tungstate hydrate was purchased from Shanghai Macklin Biochemical Co. Ltd. Ethanol was purchased from Li'Anlong Bohua (Tianjin) Pharmaceutical& Chemical Co. Ltd. Ammonia gas was purchased from Hebei Qiming New Energy Technology Co. Ltd. Reaction gas mixture (CO_2:H_2:Ar=32%:64%:4%) was purchased from Shanghai Tonghui Special Gas Co. Ltd. All solvents and chemicals were used without any further purification. Deionized water with resistivity of 18.3 MΩ•cm was used to prepare aqueous solution throughout the experiment.

Synthesis of N-W_2N_3 precursor and N-W_2N_3

The synthesis of NV-W_2N_3 precursor and NV-W_2N_3 were based on a previously developed method.[1] Riefly, 5.0 g of sodium nitrate in a crucible was heated at 350℃ for 30 min in a muffle furnace. Then 0.2 g of ammonium tungstate hydrate was added into the crucible quickly and reacted for 60 s until the sodium nitrate became molten state in the crucible. Thereafter the product was removed from the muffle furnace and cooled down to room temperature. After being washed and centrifuged with deionized water and ethanol several times the NV-W_2N_3 precursor was obtained.

500 mg of the as-prepared precursor was put into the quartz boat at the center of the tube furnace, heated to 750 °C at a heating rate of 5 °C/min under an ammonia atmosphere. The reactants were kept heating for 5 h and then cooled down to room temperature naturally. The resulting black product was washed and centrifuged with deionized water and ethanol several times until eventually dried in an oven for use.

To obtain NV-W_2N_3-2 and NV-W_2N_3-3 with more vacancy content, the above NV-W_2N_3 was annealed in 5% and 30% H_2/Ar flow to 500 °C at a heating rate of 5 °C/min, respectively. After being heated for 3 h, the reactants cooled down to room temperature naturally.

To obtain W_2N_3 without N vacancies (P-W_2N_3), the above NV-W_2N_3 was annealed in 500 °C at a heating rate of 5 °C/min, respectively. After being heated for 3 h, the reactants cooled down to room temperature naturally.

Characterization

The X-ray powder diffraction (XRD) patterns of NV-W_2N_3 nanosheets were recorded on a PANalytical X'Pert PRO powder diffractometer from ~10 to 90° 2θ using Cu Kα radiation (graphite monochromator, λ = 1.5418 Å) at room temperature.

X-ray photoelectron spectroscopy (XPS) measurements were performed on an Axis Supra instrument using a non-monochromatized Al-Kα X-ray source, and the all binding energies were calibrated by the C1s peak at 284.8 eV.

The scan scanning electron microscopy (SEM) images were collected on an Apreo field emission scanning electron microscope (FEI, USA).

The Transmission Electron Microscope (TEM) micrographs were obtained using a Talos F200S Field Emission Transmission Electron Microscopes (FEI, USA) at an operating voltage of 200 kV. Samples were dispersed onto holey carbon grids with the evaporation of excessive solvent.

The spherical aberration corrected scanning transmission electron microscopy (Cs-corrected STEM) images were obtained using Titan Themis Cubed G2 300 (FEI) microscope equipped with Super-X detectors at 300 kV.

Atomic force microscope (AFM) was used to test the thickness of NV-W_2N_3 nanosheets (Bruker Dimension Icon). When testing, the sample was dispersed and dissolved in a volatile ethanol solvent, then dropped on the silicon wafer, and performed the test after the solvent evaporated.

BET surface area, pore-volume, and pore size distribution of the catalyst were obtained from a micromeritics ASAP 2460 instrument.

The electron spin resonance (ESR) spectra were collected on a Bruker ER200DSRC10/12 spectrometer at room temperature. N vacancies between different catalysts were determined according to the method used in the previous literature.[2]

CO_2 Temperature programmed desorption (CO_2-TPD), H_2 temperature programmed reduction (H_2-TPR) and H_2 temperature programmed desorption (H_2-TPD) test

CO_2-TPD experiments were carried out on the VDSorb-91i Automated Catalyst Characterization System (Quzhou Vodo instrument Co., Ltd.) based on a previous literature[2]. First, the catalyst (317 mg) was pretreated at 300 °C for 90 min in a flow of He (15 mL/min) and then cooled down to 70 °C. After that, the catalyst was saturated with 1% CO_2/N_2 for 90 min with 30 mL/min, followed by flushing in He (30 mL/min) for 80 min to remove physical adsorbed CO_2. The CO_2-TPD measurement was carried out at 70 to 950 °C with a heating rate of 10°C/min under a continuous flow of He at 20 mL/min.

H_2-TPR experiments were also performed on the VDSorb-91i Automated Catalyst Characterization System (Quzhou Vodo instrument Co., Ltd.). First, the catalyst (11 mg) was pretreated at 300 °C for 90 min in a flow of Ar (15 mL/min) and then cooled down to 25 °C.

After that, the H_2-TPR measurement was carried out at 25 to 1000℃ with a heating rate of 10 ℃/min under a continuous flow of 10% H_2/Ar at 20 mL/min.

H_2-TPD experiments were carried out on the VDSorb-91i Automated Catalyst Characterization System (Quzhou Vodo instrument Co., Ltd.). First, the catalyst (112 mg) was pretreated at 300 ℃ for 60 min in a flow of Ar (15 mL/min) and then reduced at 300 ℃ for 60 min in a flow of 10% H_2/Ar (20 mL/min). After that, the catalyst was cooled down to 25 ℃. The catalyst was saturated with 10% H_2/Ar for 90 min with 20 mL/min, followed by flushing in Ar (30 mL/min) for 80 min to remove physical adsorbed H_2. The H_2–TPD measurement was carried out at 25 to 400 ℃ with a heating rate of 10℃/min under a continuous flow of Ar at 30 mL/min.

CO_2 hydrogenation

The CO_2 hydrogenation was carried out in a stainless steel reactor with quartz inner container (Anhui Kemi Machinery Technology Co., Ltd., Anhui, China) according to a previous report[3]. As a typical run, 60 mg of catalyst was added into the reactor. The reactor was sealed and flushed three times with 2 MPa of gas mixture to remove the air, then the CO_2/H_2/Ar gas mixture was charged in to 4.0 MPa (CO_2:H_2:Ar=32%:64%:4%, Ar gas was used as an internal standard), and the autoclave was heated to given temperature in an electric heating jacket. The temperature was measured by a thermocouple in the stainless steel reactor. After reaction, the reactor was naturally cooled down to room temperature. The gas of autoclave was collected by gas bags. The composition of gas in the autoclave was analyzed with a Fuli GC-9790 Plus gas phase chromatography (GC) equipped with thermal conductivity detector (TCD) and flame ionization detector (FID). In the recycle tests, the solid catalyst was separated by centrifugation, washed with deionized water, dried at 60°C for 3 h, and then used in the next run.

Computational Methods

The Gibbs free energy of the reaction intermediates on the catalyst and the adsorption energy of the catalyst to the intermediates were calculated based on First-principles wave-basis pseudo-potential method within density functional theory (DFT) using Generalized Gradient Approximation/Perdew-Burke-Ernzerhof (GGA/PBE) function[4, 5]. The kinetic energy cutoff was set at 450 eV and k-point mesh was 6×2×1 for the relaxation calculations. 25 Å vacuum layer in the z direction was set aside to calculate the Gibbs free energy and adsorption energy. The slab model was a four-layer W_2N_3 where the bottom two layers were fixed and the top two layers were relaxed to simulate the active surface. The basic Gibbs free energy, adsorption energy and configuration of CO_2 on the catalyst surface, etc. were calculated at 0 K, and then thermal correction was carried out at 573.15 K (300 ℃) and 4 MPa to simulate the real reaction environment.

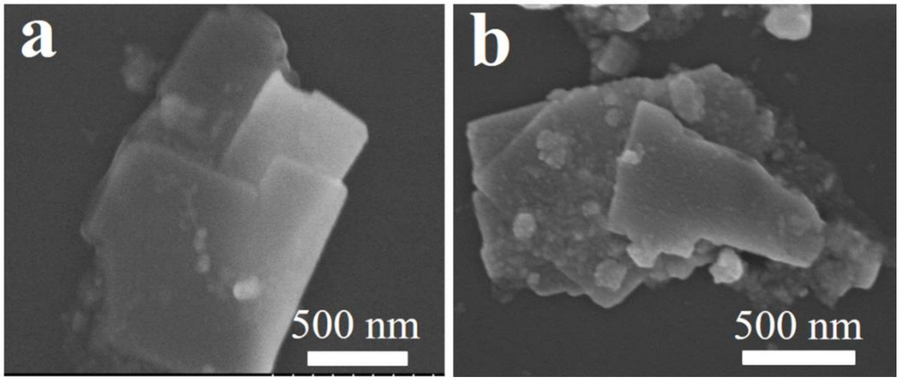

Figure S1. SEM images of the NV-W_2N_3 precursor.

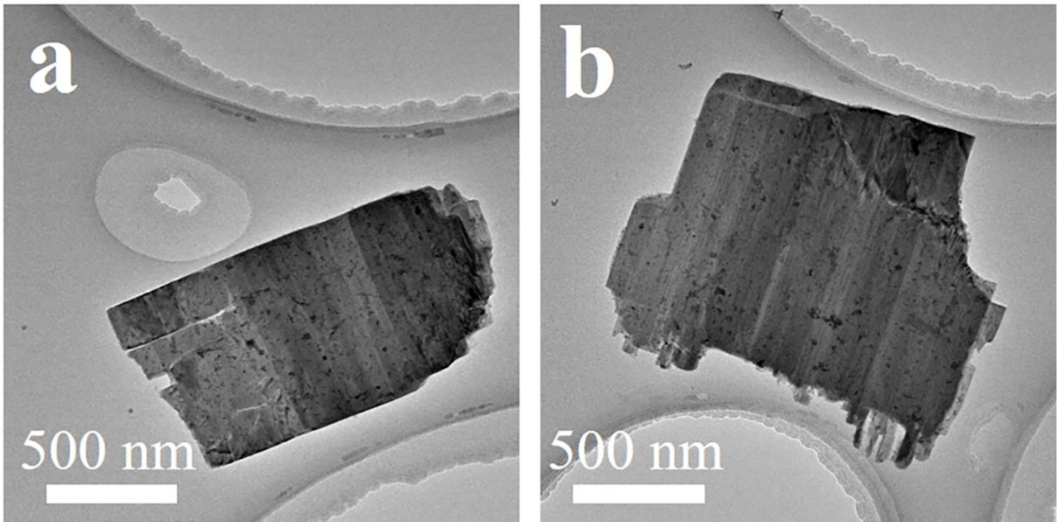

Figure S2. TEM images of the NV-W_2N_3 precursor.

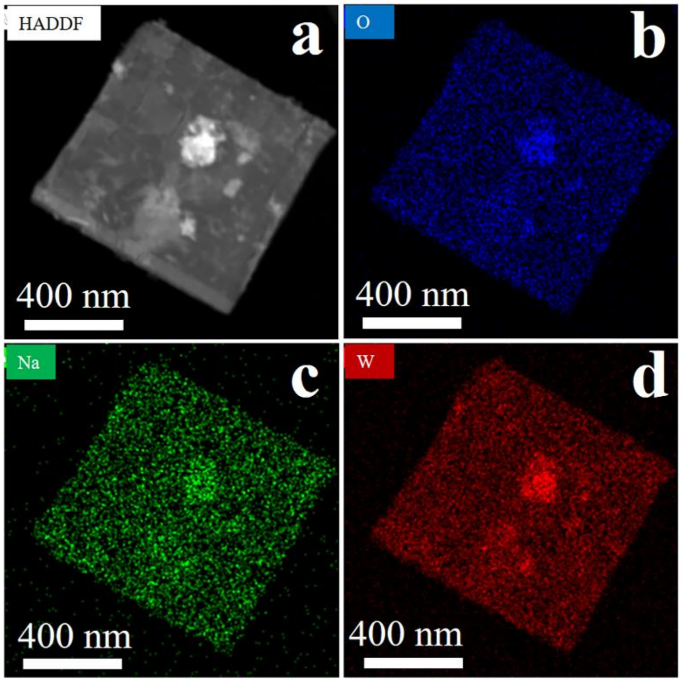

Figure S3. Element distribution mapping of the NV-W_2N_3 precursor.

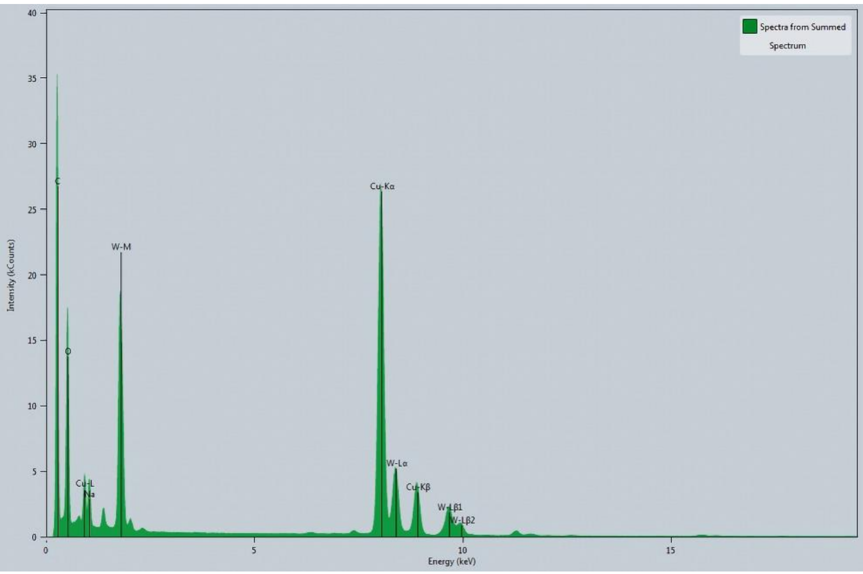

Figure S4. EDS spectra of the NV-W_2N_3 precursor.

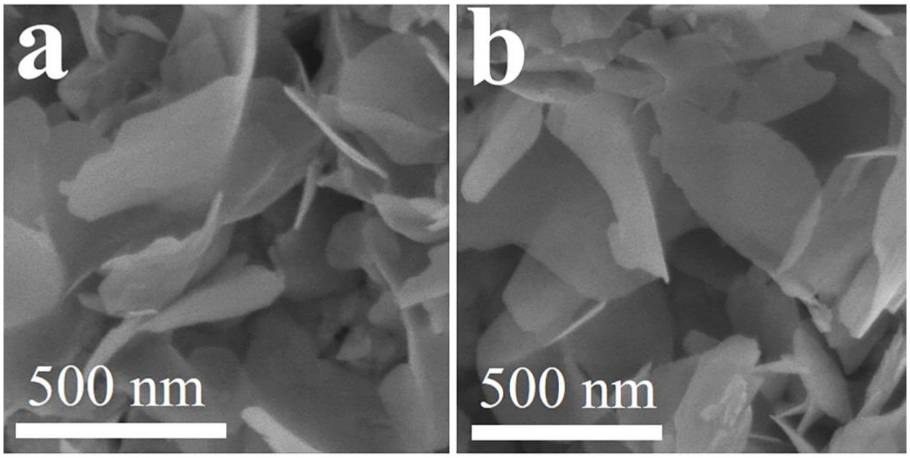

Figure S5. SEM images of the NV-W_2N_3 nanosheets.

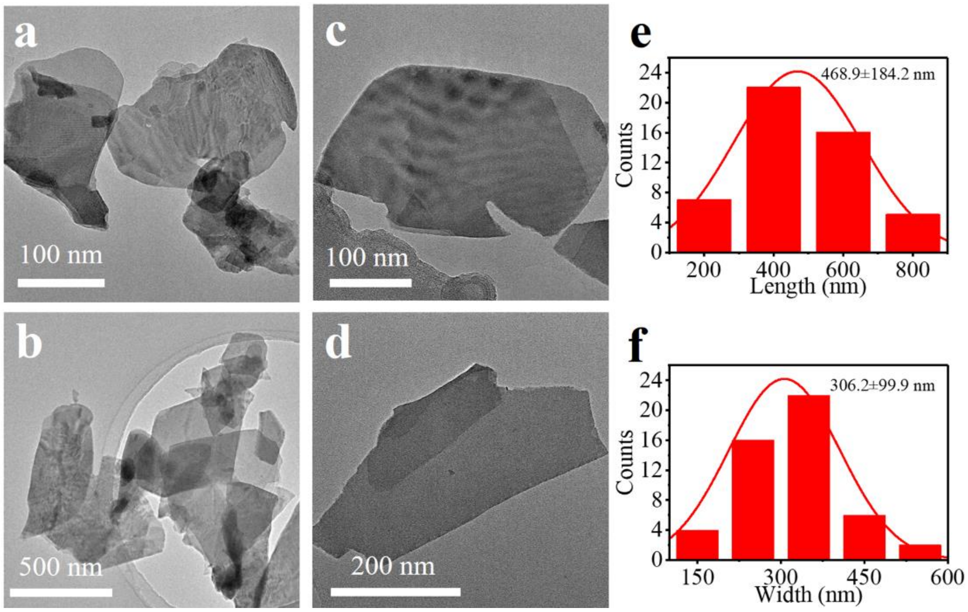

Figure S6. (a-d) More representative TEM images of NV-W_2N_3, with length of 468.9 ± 184.2 nm (e) and width of 306.2 ± 99.9 nm (f) based on the statistical data of 50 flakes.

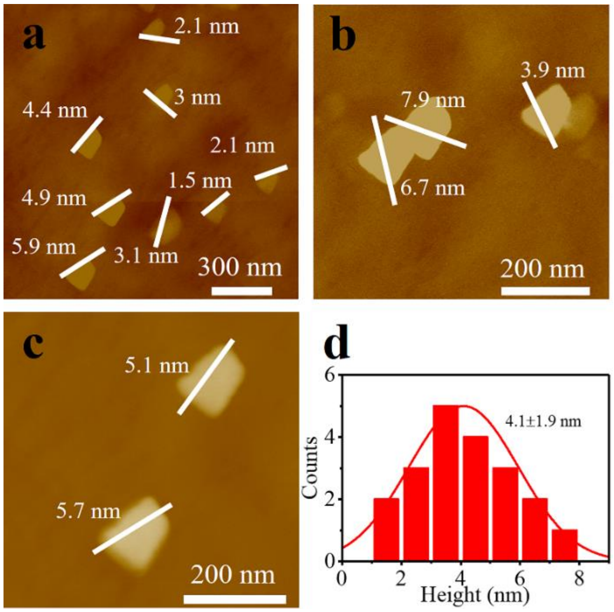

Figure S7. More representative AFM images of the NV-W_2N_3 nanosheets and the thickness statistics.

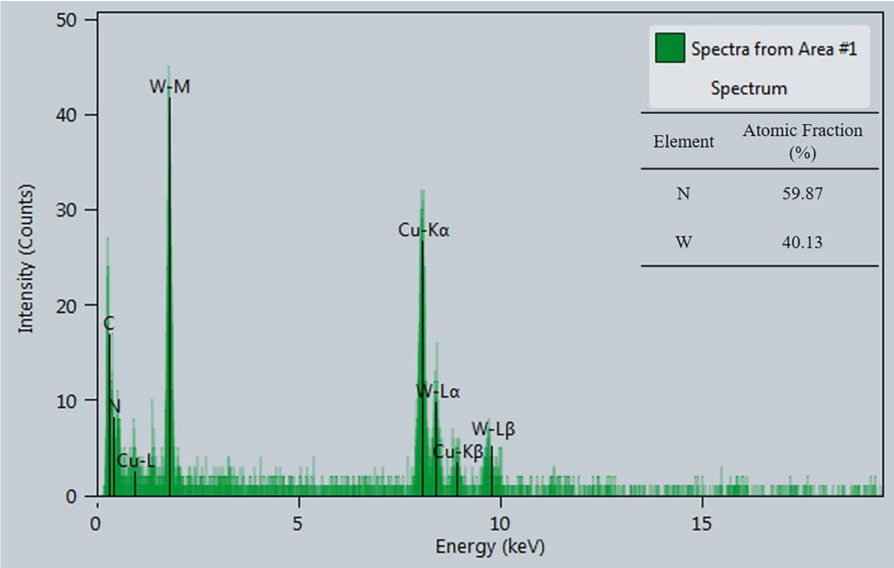

Element	Atomic Fraction (%)
N	59.87
W	40.13

Figure S8. EDS spectra of the NV-W_2N_3 nanosheets.

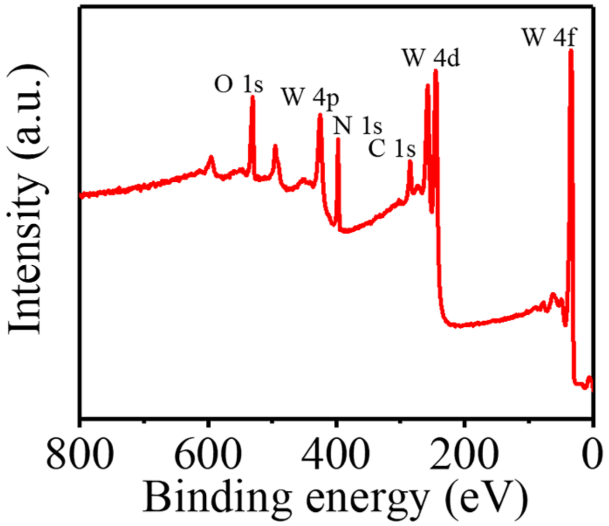

Figure S9. The XPS full spectra of NV-W_2N_3.

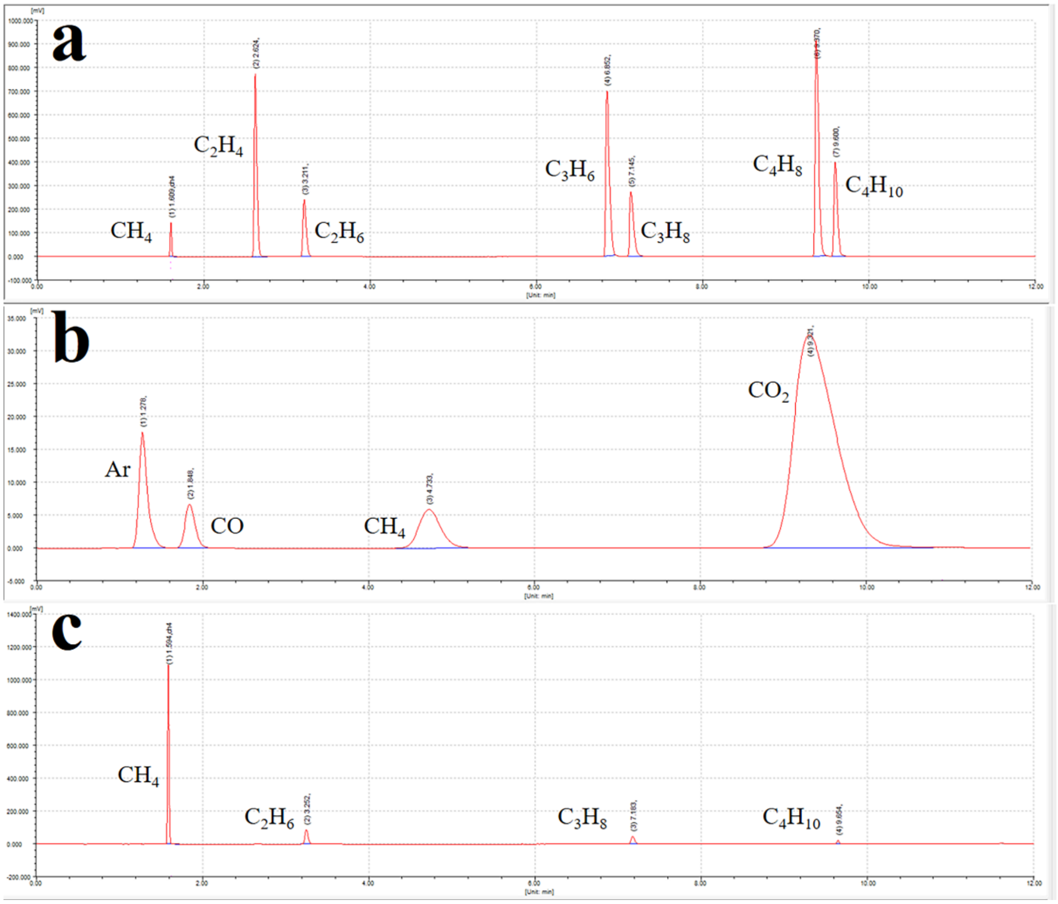

Figure S10. (a)The peaks of standard gas by FID detector in gas chromatography (CH_4: 0.997%, C_2H_4: 4.99%, C_2H_6: 2.01%, C_3H_6: 4.87%, C_3H_8: 1.98%, C_4H_8: 4.99%, C_4H_{10}: 2.01%, Ar: balance). (b) The peaks of CO_2 hydrogenation products by TCD detector in gas chromatography. (c) The peaks of CO_2 hydrogenation products by FID detector in gas chromatography.

Table S1. Comparison of the catalytic performance of NV-W_2N_3 in this work and previously reported catalysts.

Catalyst	P (MPa)	H_2/CO_2	T (°C)	WHSV ($mLg^{-1}h^{-1}$)	CO_2 Conversion (%)	Selectivity (%)					Ref.
						CO	CH_4	MeOH	C_{2+}	DME	
NV-W_2N_3	4	2	300	-	24	23	54	-	23	-	**This work**
GaN	2	2	360	3000	7.5		-	18	6	76	Nat. Commun. 2021, 12, 2305.
$Fe_2N@C$	1	4	250	-	33.7	15.8	38.8	-	45.4	-	Angew. Chem.-Int. Edit. 2021, 60, 4496-4500.
2D-Mo_2C	2.5	3	430	-	36	39	51	-	10	-	Nat. Commun. 2021, 12, 5510.
Co/MXene		4	400	24000	32.2	13.6	62.6	-	-	-	Small 2021, 17, 2007509.
FL-MoS_2	5	3	180	3000	12.5	2	3.7	94.3	-	-	Nat. Catal. 2021, 4, 242-250.
Fe/SiO_2	1	3	300	3600	6.2	70	23	-	7	--	ACS Catal. 2021, 11, 6175-6185.
FeK/Co−NC	2.5	3	300	-	34	12	12	-	76	-	ACS Catal. 2021, 11, 2267-2278.
Na−$CoFe_2O_4$ /CNT	1	3	340	3600	34.4	18.6	12	-	69.4	-	ACS Catal. 2020, 10, 8660-8671.
10%Mn-FeNa	0.5	3	290	20000	22.8	53.5	22.8	-	23.7	-	J. Catal. 2020, 390, 12-22.
FeK/MWNTs	2	3	340	9000	43.6	23.4	20.8	-	55.8	-	ACS Catal. 2020, 10, 6389-6401.
$FeAlO_x$-5	3.5	1	330	2000	20.2	16.8	4.5	--	78.7	-	ACS Catal. 2020, 10, 10325-10338.
In_2O_3-$ZnZrO_x$ /SAPO-34-C	3	3	380	9000	18.1	52.5	0.6	-	46.9	-	Chemsuschem 2019, 12, 3582-3591.

$ZnGa_2O_4$ / SAPO-34	3	3	370	54000	13	46	0.5	-	53.5	-	Chem. Commun. 2018, 54, 140-143.
Ni@Au/SiO_2	1	3	600	60000	18	95	5	-	-	-	Nat. Catal. 2020, 3, 411-417.
Rh@S-1	1	3	500	-	51.6	20.2	79.8	-	-	-	J. Am. Chem. Soc. 2019, 141, 8482-8488.
$CoZrO_x$ (10)	3	4	340	10000	19	95		5			ACS Catal. 2021, 11, 9450-9461.
c-In_2O_3-S	5	3	300	9000	12.0	28.1	-	71.9	-		Sci. Adv. 6, eaaz2060.
Co@$Si_{0.95}$	2	3	320	6000	8.6	20.5	9	70.5	-		Nat. Commun. 2020, 11, 1033.

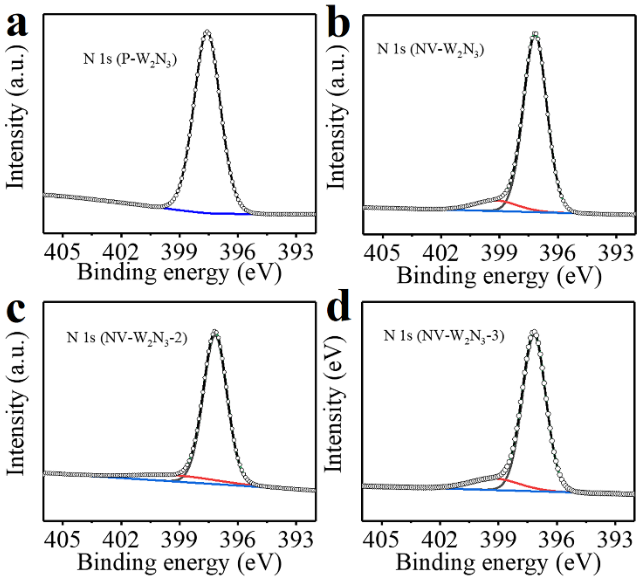

Figure S11. (a) The N 1s spectra of the P-W_2N_3 (a), NV-W_2N_3 (b), NV-W_2N_3-2 (c) and NV-W_2N_3-3 (d).

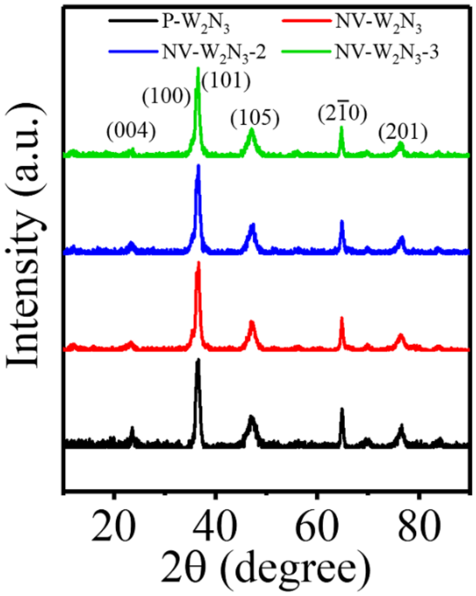

Figure S12. The XRD patterns of the P-W_2N_3, NV-W_2N_3, NV-W_2N_3-2, NV-W_2N_3-3 catalysts.

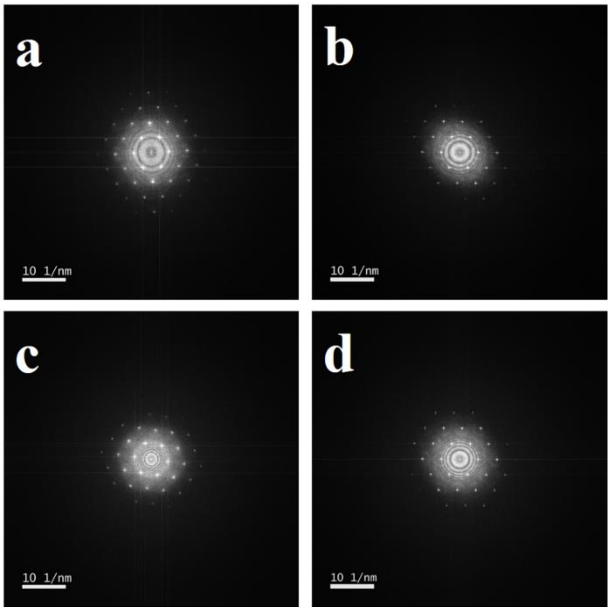

Figure S13. The SAED patterns (obtained by FFT analysis) of (a) P-W_2N_3, (b) NV-W_2N_3, (c) NV-W_2N_3-2 and (d) NV-W_2N_3-3.

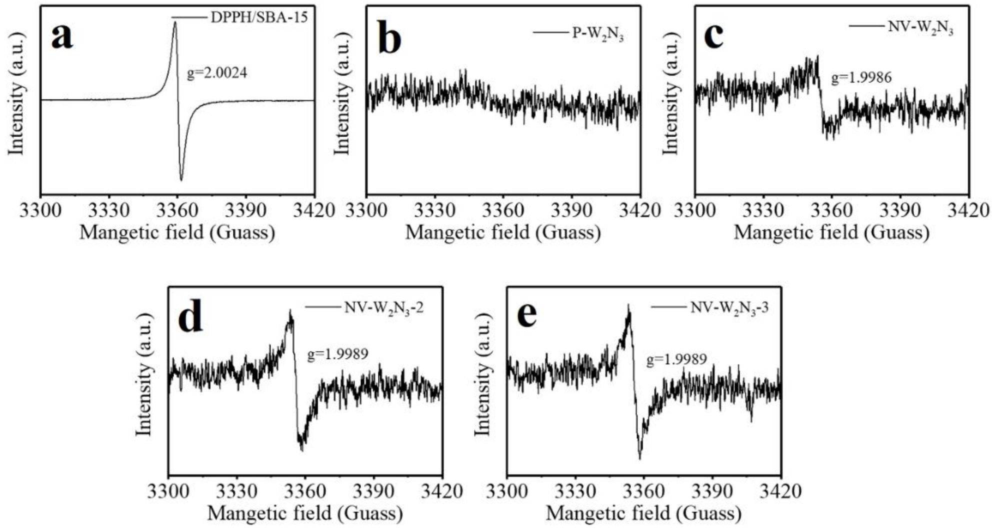

Figure S14. The ESR spectra of (a) 1,1-Diphenyl-2-picryl-hydrazyl (DPPH)/SBA-15 (as an internal standard), (b) P-W_2N_3, (c) NV-W_2N_3, (d) NV-W_2N_3-2 and (e) NV-W_2N_3-3.

Table S2. A comprehensive comparison of CO_2 hydrogenation efficiency in association with catalyst N vacancies.

		P-W_2N_3	NV-W_2N_3	NV-W_2N_3-2	NV-W_2N_3-3
CO_2	Conversion (%)	18.04	24.16	25.28	26.21
Selectivity (%)	CO	24.65	22.98	24.29	25.07
	CH_4	51.99	54.48	55.55	57.41
	C_{2+}	23.36	22.52	20.16	17.52
N vacancy population via ESR (mol/g)		/	7.63×10^{-7}	7.99×10^{-7}	9.16×10^{-7}
N vacancy population via XPS (The area ratios of vacancy peaks in N peaks (%))		0	10.02	12.83	13.47

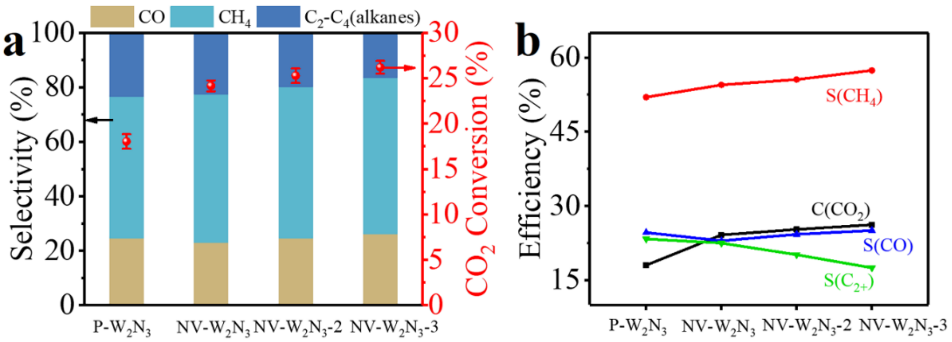

Figure S15. The performance of the P-W_2N_3, NV-W_2N_3, NV-W_2N_3-2, NV-W_2N_3-3 catalysts in the hydrogenation of CO_2 shown in histograms (a) and line charts (b).

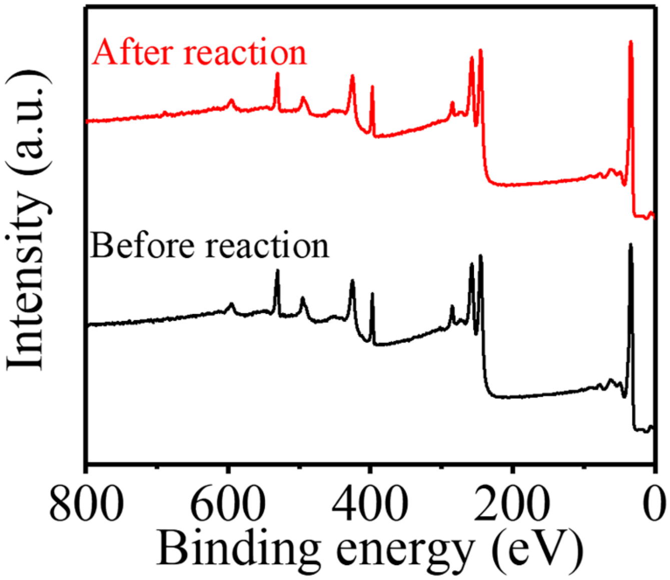

Figure S16. The XPS spectra of the NV-W_2N_3 nanosheets before and after catalytic reaction.

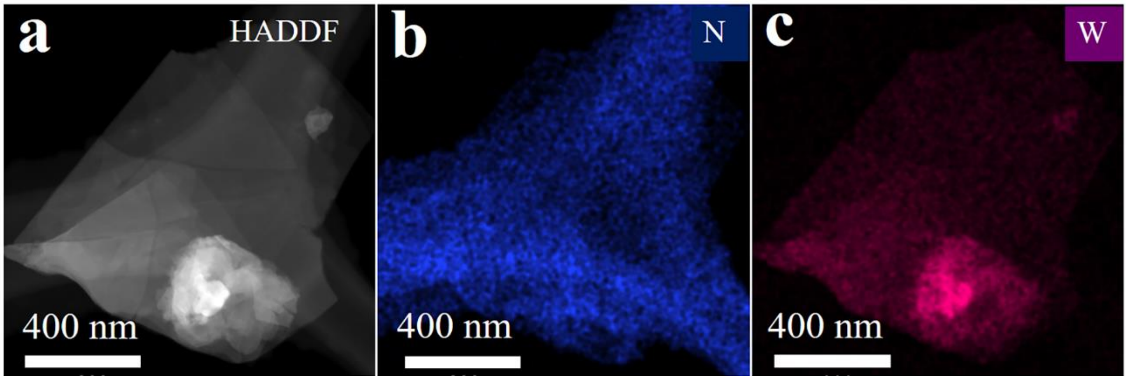

Figure S17. Element distribution mapping of the NV-W_2N_3 nanosheets after reaction.

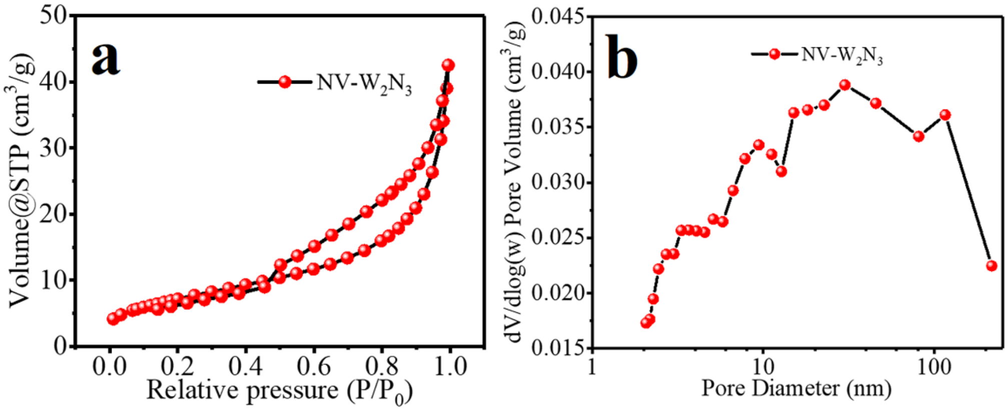

Figure S18. (a) Nitrogen adsorption-desorption isotherms, and (b) pore size distribution of NV-W_2N_3.

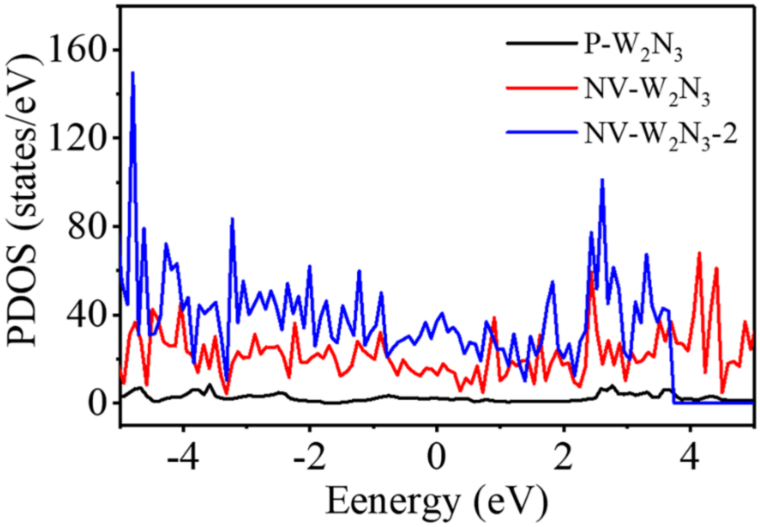

Figure S19. The density of states (DOS) diagrams of P-W_2N_3 (without vacancies in the exposed crystal plane), NV-W_2N_3 (with 1 vacancy in the exposed crystal plane) and NV-W_2N_3-2 (with 2 vacancies in the exposed crystal plane).

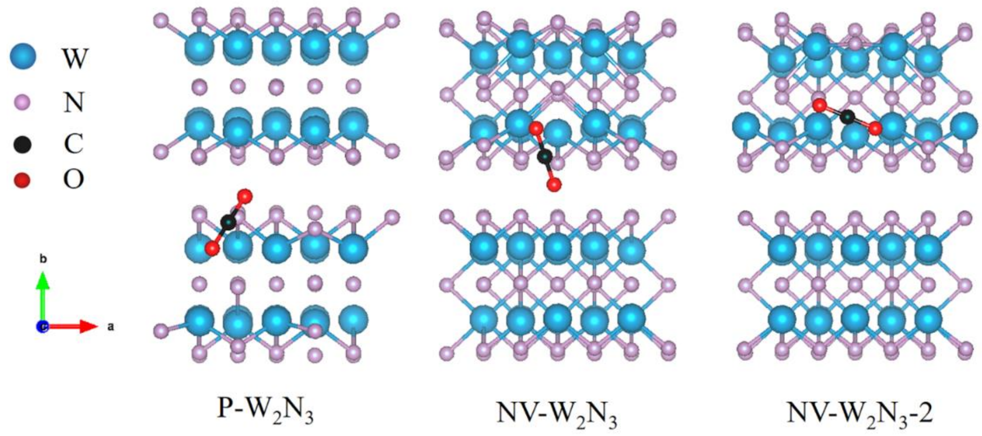

Figure S20. The calculated configuration of CO_2 on P-W_2N_3, NV-W_2N_3 and NV-W_2N_3-2.

Table S3. The adsorption energy of CO_2 molecule on P-W_2N_3, NV-W_2N_3 and NV-W_2N_3-2.

Catalyst	Adsorption energy (eV)
P-W_2N_3	-25.81
NV-W_2N_3	-23.05
NV-W_2N_3-2	-24.43

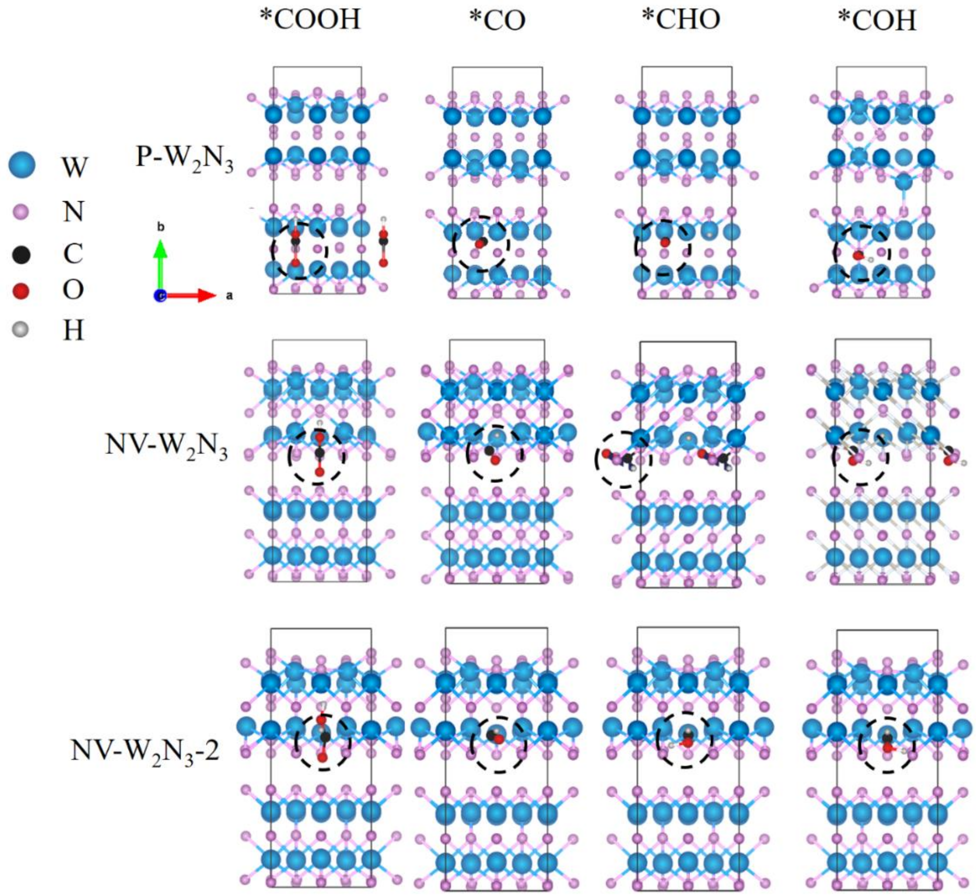

Figure S21. The specific calculation models of intermediates for P-W$_2$N$_3$, NV-W$_2$N$_3$ and NV-W$_2$N$_3$-2.

Table S4. The Gibbs free energy of the main reaction intermediates.

Intermediates	Gibbs free energy (eV)[a]	Gibbs free energy (eV)[b]	Gibbs free energy (eV)[c]
*COOH	-2.44	-1.22	-1.54
*CO	-2.09	-1.64	-1.58
*COH	-1.57	-1.45	-1.16
*CHO	-2.63	-3.18	-2.88

a. Gibbs free energy of intermediates on P-W_2N_3.

b. Gibbs free energy of intermediates on NV-W_2N_3.

c. Gibbs free energy of intermediates on NV-W_2N_3-2.

Table S5. The adsorption energy of *COH and *CHO.

Intermediates	Adsorption energy (eV) [a]	Adsorption energy (eV) [b]	Adsorption energy (eV) [c]
*CHO	-3.28	-3.84	-3.54
*COH	-1.45	-1.34	-1.05

a. Adsorption energy of intermediates on the P-W_2N_3.

b. Adsorption energy of intermediates on the NV-W_2N_3.

c. Adsorption energy of intermediates on the NV-W_2N_3-2.

References

(1) Jin, H. Y.; Li, L. Q.; Liu, X.; Tang, C.; Xu, W. J.; Chen, S. M.; Song, L.; Zheng, Y.; Qiao, S. Z. Nitrogen Vacancies on 2D Layered W_2N_3: a Stable and Efficient Active Site for Nitrogen Reduction Reaction. *Adv. Mater.* **2019**, *31*, 1902709.

(2) Feng, W. H.; Yu, M. M.; Wang, L. J.; Miao, Y. T.; Shakouri, M.; Ran, J. Q.; Hu, Y. F.; Li, Z. Y.; Huang, R.; Lu, Y. L.; et al. Insights into Bimetallic Oxide Synergy during Carbon Dioxide Hydrogenation to Methanol and Dimethyl Ether over $GaZrO_x$ Oxide Catalysts. *ACS Catal.* **2021**, *11*, 4704-4711.

(3) Wang, L.; Wang, L.; Zhang, J.; Liu, X.; Wang, H.; Zhang, W.; Yang, Q.; Ma, J.; Dong, X.; Yoo, S. J.; et al. Selective Hydrogenation of CO_2 to Ethanol over Cobalt Catalysts. *Angew. Chem., Int. Ed.* **2018**, *57*, 6104-6108.

(4) Perdew, J. P.; Ruzsinszky, A.; Csonka, G. I.; Vydrov, O. A.; Scuseria, G. E.; Constantin, L. A.; Zhou, X.; Burke, K. Restoring the Density-gradient Expansion for Exchange in Solids and *Surfaces. Phys. Rev.* Lett. **2008**, *100*, 136406.

(5) Milman, V.; Winkler, B.; White, J. A.; Pickard, C. J.; Payne, M. C.; Akhmatskaya, E. V.; Nobes, R. H. Electronic Structure, Properties, and Phase Stability of Inorganic Crystals: a Pseudopotential Plane-wave Study. *Int. J. Quantum Chem.* **2000**, *77*, 895-910.